

1 **On the Inefficiency of Moist Geostrophic Turbulence: A Theory for the**
2 **Energetic Output under Sub-saturated Conditions**

3 Marguerite Brown^a, Olivier Pauluis^b, and Edwin P. Gerber^b

4 ^a *Université du Québec à Montréal, Montreal, QC*

5 ^b *Center for Atmosphere Ocean Science, Courant Institute of Mathematical Sciences, New York*
6 *University, New York NY*

7 *Corresponding author: Marguerite Brown, brown.marguerite_lynnette@uqam.ca*

8 *Current affiliation: UQAM, Montreal, QC.*

9 ABSTRACT: The midlatitude stormtracks have traditionally been understood as driven by the
10 meridional transport of sensible heat down the Equator-to-Pole temperature gradient. However,
11 latent heat accounts for an estimated 30-60% of the meridional energy transport, a portion which
12 is likely to increase under warming. The contribution of latent heat to the total energetics is
13 complicated in that it is inefficient: only a portion of the transported latent heat is converted into
14 kinetic energy. Currently, there is no complete theory for what sets the relationships between
15 meridional energy transport and kinetic energy generation by midlatitudes eddies. We use a
16 two-layer moist quasi-geostrophic model to develop the theory of how the energetic output of
17 the midlatitude atmosphere depends on the relative humidity structure. By tuning the surface
18 evaporation rate, we show that the system reaches a maximum energetic output in the saturated
19 limit, with great reductions at lower evaporation rates. We quantify these reductions in terms of
20 a moist conversion efficiency. Using a Moist Energetic framework, we identify that precipitation
21 dissipation and the diffusion of moisture in subsaturated regions account for the reduction in
22 energetic output. We then show that the moist conversion efficiency can be predicted by the
23 distribution of humidity.

24 SIGNIFICANCE STATEMENT: The impact of humidity on the strength of mid-latitude storms
25 is not well understood. Humidity will increase as the planet warms, but it is unclear whether
26 storms will become stronger or weaker as a result. We use an idealized computer model to learn
27 about how humidity will impact the strength of storms. We focus on the effect of evaporation at
28 the planet’s surface, with simulations ranging from a completely dry atmosphere to one with rain
29 everywhere. In between these two limits, it is raining in only part of the atmosphere and storms
30 are much weaker than the case with rain everywhere. We discuss how to connect these results to
31 more complex models and real-world data.

32 1. Introduction

33 Predicting the intensity of midlatitude stormtracks presents an ongoing challenge in climate fore-
34 casting. Models have underestimated both the intensification of stormtracks under warming and
35 the transport of moist static energy across them, particularly in the Southern hemisphere (Chemke
36 et al. 2022). This occurs despite relatively constant hemispheric temperature gradients and baro-
37 clinicity, which are traditionally understood as the primary drivers of storms in the midlatitudes.
38 Hemispheric humidity gradients, however, increase by $\sim 7\%$ per K. Because humidity and tem-
39 perature interact when latent heat is released through condensation, moist processes contribute to
40 a tug-of-war on the eddy kinetic energy (EKE) of the stormtracks (Shaw et al. 2016), with some
41 factors contributing to increases and others to decreases. These opposing influences mean that the
42 impact of moisture on the size, frequency, and propagation of storms can change, even if latent
43 heat is not the primary driver of changes to the total energetics (e.g., Lorenz and DeWeaver 2007;
44 O’Gorman 2010). An updated theory including the impact of moisture is necessary to understand
45 the total effect.

46 This study develops a theory for how moisture impacts the kinetic energy of the midlatitude
47 atmosphere, with an emphasis on how the relative humidity of the atmosphere limits mechanical
48 output. We use an idealized framework, the Moist Quasi-geostrophic model (MQG) of Lapeyre
49 and Held (2004), which is particularly well-suited for our purpose as it features a uniform back-
50 ground evaporation that tunes the relative humidity. Our first paper Brown et al. (2023) discusses
51 the energetics of MQG under very high evaporation, keeping the atmosphere at saturation nearly
52 everywhere. Our analysis introduced the concept of Moist Energy (ME), a quadratic term quan-

53 tifying moisture fluctuations. In the saturated limit, downgradient moisture transport acts as a
54 source for the Eddy Moist Energy (EME), which is converted into EKE, with more intense eddies,
55 a stronger inverse cascade, and a larger eddy-containing scale than a dry atmosphere with the same
56 meridional temperature gradient.

57 However, as precipitation only occurs over a small fraction of the atmosphere, this saturated
58 limit is unlikely to capture the full extent of the impacts of moisture in the energetics of the
59 stormtracks. The original experiments of Lapeyre and Held (2004) use a lower evaporation
60 rate and, consequently, feature large unsaturated regions. We argue that the energetics of moist
61 geostrophic turbulence depend not only on the moisture and temperature gradients, but also on
62 the portion of the domain that is unsaturated. We consider a wider range of evaporation rates to
63 explore the transition from low to high relative humidity and address the question: how does the
64 injection of energy through evaporation (latent heat) at the surface impact the production of kinetic
65 energy? In particular, how does this transition vary with the strength of background gradients in
66 temperature and moisture? We define and develop a *moist conversion efficiency* as a measure of
67 how moisture gradients are converted into EKE, as compared with the saturated case which we
68 take to be full efficiency. We show that the moisture gradient efficiency increases rapidly at low
69 evaporation, then gradually converges to a saturated limit at high evaporation. We further explore
70 how moist systems lose EME through small-scale diffusion and dissipation due to moist processes.

71 Section 2 discusses the background pertaining to the impact of moisture on midlatitude atmo-
72 spheric dynamics. In Section 3, we review the MQG system and discuss the underlying energetic
73 framework, with an emphasis on the generation and dissipation of EME. Section 4 investigates how
74 mechanical efficiency manifests itself in MQG. Section 5 defines moisture conversion efficiency
75 and the mechanisms that contribute to it. Section 6 synthesizes the results of the previous section
76 and introduces a parameter that is predictive of the moisture conversion efficiency. Section 7
77 concludes the study.

78 **2. Background**

79 In this work, we focus on how moisture impacts energetics using intuition from "dry" geostrophic
80 theory. The atmosphere acts as a heat engine, generating kinetic energy through the downgradient
81 transport of heat. In the tropics, this manifests as energy transport from the warm surface to the cold

82 top of the atmosphere. The midlatitudes additionally feature a significant meridional temperature
83 gradient, resulting in a redistribution of heat from the tropics to the poles. The result is a baroclinic
84 system with synoptic-scale storms, the intensity of which is constrained by the efficiency of the
85 mid-latitude heat engine (e.g., Barry et al. 2002).

86 To translate this intuition to a moist framework, we need two key adjustments. First, the heat
87 transport must include latent heat. In the current climate, latent heat accounts for between one-third
88 and one-half of the poleward energy transport in the midlatitudes, a portion expected to increase in
89 a warmer world. Second, the introduction of moisture fundamentally affects the efficiency of heat
90 engines. Pauluis (2011) shows that the mechanical output of the thermodynamic cycle involving
91 moist air is greatly constrained by the degree of saturation in the cycle. A saturated cycle - one
92 where the system is everywhere at the saturation value set by Clausius-Clayperon - generates the
93 same mechanical output as a Carnot cycle. A partially saturated cycle is significantly less efficient.
94 Evaporation of water vapor in unsaturated air, diffusion of water vapor, and falling rainfall are
95 irreversible processes that can greatly reduce the mechanical output of a moist atmosphere. This
96 effect has been demonstrated for convection (Pauluis and Held 2002a,b; Singh and O’Gorman
97 2016; Lever and Pauluis 2024), tropical cyclones (Pauluis and Zhang 2017), and the general global
98 circulation (Laliberté et al. 2015).

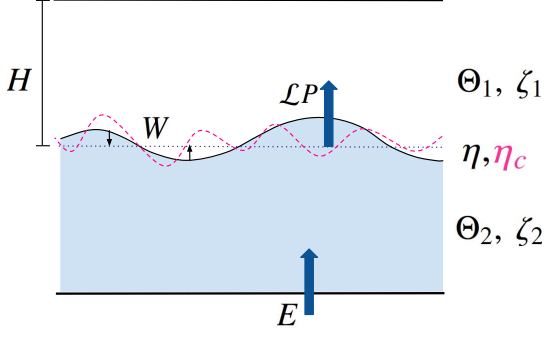
99 A theory for moist geostrophic turbulence must address these two aspects - the enhancement
100 of the meridional heat transport by the inclusion of latent heat and the reduction of mechanical
101 output due to moist processes. Indeed, moisture has been observed to have competing effects
102 on processes relevant to the midlatitude storm tracks. Moisture can intensify instabilities by
103 reducing the effective stratification for ascending parcels (Emanuel et al. 1987; Lapeyre and Held
104 2004; Lambaerts et al. 2011; Schneider and O’Gorman 2008). The theory behind these localized
105 instabilities has primarily been developed in linearized systems with highly parameterized moisture
106 that is assumed to be continuously available without an explicit evaporation term. These studies
107 have provided useful insights into the scale, growth, and evolution of such instabilities (Whitaker
108 and Davis 1994; Parker and Thorpe 1995; Moore and Montgomery 2004; Adames and Ming 2018;
109 Kohl and O’Gorman 2022) that are borne out well in mesoscale models (Moore and Montgomery
110 2005), GCMs (O’Gorman et al. 2018), and reanalysis data (Wernli et al. 2002; Moore et al.
111 2008). However, they provide limited insight into how the availability of moisture, governed by

112 planetary constraints such as the evaporation rate and poleward transport of latent heat, determine
113 the frequency of such instabilities.

114 For equilibrated systems (e.g. radiative-convective equilibrium, quasi-equilibrium), moisture
115 weakens the flow. In the midlatitudes, the poleward transport of latent heat reduces EKE by
116 changing the temperature structure of the atmosphere. This effect is especially pronounced in
117 the presence of a non-homogeneous background gradient, e.g. a Bickley jet, where precipitation
118 poleward of the jet flattens the meridional temperature gradient (Bembenek et al. 2020; Lutsko and
119 Hell 2021). Furthermore, when changes to the dry static stability at least partially compensate for
120 the destabilizing effect of a moister atmosphere (Juckes 2000; Zurita-Gotor 2005; Frierson 2006),
121 moist baroclinic growth occurs less frequently, restricting the growth of EKE on average over long
122 time periods.

123 We propose that the combined effect of moisture on the midlatitude stormtracks depends on
124 the question of how efficiently moisture gradients are converted into EKE as a function of mean
125 moisture deficit. Indeed, the initial distribution of moisture has been shown to significantly impact
126 the total energetics in eddy life-cycles (Pavan et al. 1999). Implicitly underlying this result is
127 the interplay between the generation of small-scale moisture variance by turbulent mixing and its
128 removal by diabatic processes. We show that the portion of the domain at saturation influences the
129 energetics of the system by determining the predominant process by which moisture anomalies are
130 removed. Subsaturated regions tend to mix moisture to smaller scales, resulting in the removal of
131 moisture anomalies by dissipation. This same process can result in highly localized condensation
132 and the formation of isolated vortices. In contrast, highly saturated systems tend to convert
133 moisture anomalies into temperature anomalies at scales larger than the turbulent dissipation scale.
134 Consequently, the degree of saturation determines the mechanical output of moist geostrophic
135 turbulence.

136 In Brown et al. (2023), we focused on how the inclusion of the meridional latent heat transport
137 greatly enhanced geostrophic turbulence in the saturated limit. Using MQG with high evaporation
138 and fast precipitation adjustment, we found that steeper moisture gradients corresponded with a
139 significant increase in the generation of kinetic energy and an elongation of the inverse cascade of the
140 barotropic flow. This first study focused solely on the limiting case of a saturated atmosphere with
141 precipitation occurring everywhere. This had the advantage of being mathematically equivalent



146 FIG. 1. The Moist Quasi-Geostrophic model of Lapeyre and Held (2004), consisting of a top and bottom
 147 layer vorticity ζ_i , $i = 1, 2$ respectively, an interface thickness η , and a condensation thickness η_c . The moisture
 148 is contained to the bottom layer, shaded blue, and precipitation P occurs when the moisture content rises above
 149 the condensation thickness, depicted by the dashed magenta line. Vertical motion W adjusts interface anomalies
 150 to a reference value. A constant evaporation rate E replenishes the moisture content of the bottom layer, and
 151 radiative cooling R raises the interface η and the condensation interface η_c .

142 to a dry model after a rescaling based on the vertical and meridional moisture gradients, but
 143 also circumvented the more difficult issue of how much kinetic energy is generated in a partially
 144 saturated atmosphere. We aim to address the latter question.

145 3. Model Description

152 As in Brown et al. (2023), we use the Moist Quasi-Geostrophic (MQG) model of Lapeyre and
 153 Held (2004) (Figure 1), a two-layer model on a β plane with moisture constrained to the bottom
 154 layer. The evolution of the system is described by the equations

$$\frac{D_1}{Dt} (\zeta_1 + \beta y) = -f_0 \frac{W}{H} - \nu \nabla^8 \zeta_1, \quad (1)$$

$$\frac{D_2}{Dt} (\zeta_2 + \beta y) = +f_0 \frac{W}{H} - r \zeta_2 - \nu \nabla^8 \zeta_2, \quad (2)$$

$$\frac{D_2}{Dt} \eta = -W + \mathcal{L}P - R - \nu \nabla^8 \eta, \quad (3)$$

$$\frac{D_2}{Dt} \eta_c = -\frac{\mathcal{L}P}{\mu_s - 1} + \frac{E - R}{1 + C} - \nu \nabla^8 \eta_c, \quad (4)$$

$$P = \begin{cases} 0 & \eta \geq \eta_c \\ (1 + C) \frac{\eta_c - \eta}{\tau} & \eta < \eta_c \end{cases}. \quad (5)$$

155 We decompose the flow into the top and bottom layer vorticity (ζ_1 and ζ_2 , respectively). The
156 material derivative of the i th layer flow is represented with D_i/Dt . Each vorticity is advected
157 by the flow in its own layer, while the interface η and condensation interface η_c are advected by
158 the lower layer. The first term on the right-hand side of the vorticity equations Equations (1)
159 and (2) captures the generation of vertical motion by ageostrophic convergence and divergence
160 $W = H\nabla \cdot \vec{u}_1$, which can be assessed diagnostically through an Omega equation (see Appendix
161 B of Brown et al. 2023). The second term on the right hand side of Equation (2) is the Ekman
162 dissipation at the surface. The final term in all prognostic equations is a higher order numerical
163 dissipation.

164 Equation (3) captures the evolution of the interface between the two layers, at a position $z =$
165 $H - \eta$. In quasi-geostrophic (QG) theory, η is proportional to the baroclinic streamfunction
166 $\psi_1 - \psi_2$ via the thermal wind relation $\eta = H(\psi_1 - \psi_2) / \lambda^2 f_0$. The Rossby deformation radius
167 $\lambda = \sqrt{g^* H / f_0}$ is defined in terms of the effective gravity $g^* = g\delta\theta/\theta_0$, the reference thickness H ,
168 and the reference rotation rate f_0 . Under the assumption that moisture is confined to the lower
169 layer, the interface position η also characterizes the maximum vertical extent of water vapor. The
170 interface is additionally forced by latent heat release in response to precipitation P and dissipated
171 by a constant radiative cooling R . The strength of latent heating relative to the vertical stratification
172 is characterized by the non-dimensional parameter $\mathcal{L} = \frac{L_q m_0}{c_p \delta\theta}$, where L_q is the strength of latent
173 heating, m_0 is a reference moisture content, and c_p is the specific heat capacity at constant pressure.

174 Following Brown et al. (2023), Equation (4) introduces the condensation thickness η_c , constructed
175 as a moisture equation independent of ageostrophic convergence. The condensation height is
176 defined by

$$\eta_c = \eta + \frac{m - C\eta}{1 + C}. \quad (6)$$

177 Here, m is a thickness-equivalent water vapor mixing ratio, defined relative to a reference value m_0
178 such that the total mixing ratio is given by $m_0 (1 + m/H)$. This moisture is contained in the bottom
179 layer, governed by the equation

$$\frac{D_2}{Dt} m = +W - P + E. \quad (7)$$

180 The mixing ratio is increased by ageostrophic convergence W in the lower layer, removed by
 181 precipitation P , and continuously replenished by evaporation E from the surface. The evaporation
 182 is constant, such that $R = \mathcal{L}E$.

183 Precipitation occurs when the moisture content exceeds a saturation value. We define the
 184 saturation value m_s by a linearization of the Clausius-Clayperon relation, such that

$$m_s = C\eta. \quad (8)$$

185 Equivalently, in the regions where the moisture content, bounded by η (the solid black line in
 186 Figure 1) rises above the condensation level η_c (the dotted pink line in Figure 1), the system is
 187 supersaturated (see Figure 2 of Brown et al. (2023)). When supersaturation occurs, precipitation P ,
 188 determined in Equation (5), relaxes the condensation level to the interface level with characteristic
 189 time τ .

190 Precipitation results in a reduction in the effective static stability of the system. The strength
 191 of this reduction is determined by the strength of latent heat release. Since moisture surpluses
 192 arise from both the vertical and meridional transport of moisture, the stratification reduction at
 193 saturation is defined relative to both the vertical and meridional moisture gradients, as

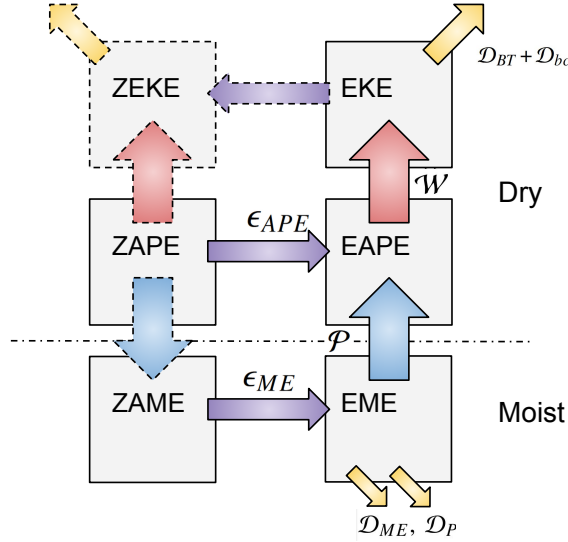
$$\mu_s^{-1} = \frac{1 - \mathcal{L}}{1 + C\mathcal{L}}. \quad (9)$$

194 Each prognostic equation contains an eighth-order diffusion term dominant at small scales. As
 195 we show, this term is a significant sink of the condensation thickness. In all other terms, it acts to
 196 enforce numerical stability and is negligible.

197 Both the interface and the condensation level have a homogenous background gradient,

$$\bar{\eta} = \bar{\eta}_c = -U\lambda^{-2}y, \quad (10)$$

198 where U is a reference wind shear. Equivalently, the background meridional moisture gradient
 199 is proportional to the temperature gradient by the Clausius-Clayperon coefficient C . Classic dry



203 FIG. 2. A modified Lorenz cycle for the MQG system. In the classical dry Lorenz cycle of a homoge-
 204 neous two-layer QG system, depicted above the dot-dashed line, Eddy Available Potential Energy (EAPE) is generated when
 205 the downgradient flux of the thickness (ϵ_{APE}) converts the zonally-averaged ZAPE into EAPE, respectively. The
 206 EAPE is converted into EKE through vertical motions and lost through Ekman Dissipation (\mathcal{D}_E). The dashed
 207 borders indicate terms that would be included in the full Lorenz cycle, but do not impact in our QG model.
 208 Moisture modifies this cycle through the injection of precipitation \mathcal{P} into the APE. However, this transfer
 209 accounts for only a portion of the EME generated from the ZAME by the downgradient flux of the condensation
 210 thickness (ϵ_{ME}). The remainder of the EME is lost through small scale-diffusion \mathcal{D}_{ME} and eddy precipitation
 211 dissipation \mathcal{D}_P . These losses reduce the mechanical efficiency of the full moist system.

200 baroclinic theory predicts unstable growth when the criticality ξ exceeds a critical value, i.e.

$$\xi \equiv \frac{U}{\lambda^2 \beta} > 1. \quad (11)$$

201 The saturated theory predicts unstable growth based on a saturated criticality,

$$\mu_s \xi \equiv \mu_s \frac{U}{\lambda^2 \beta} > 1, \quad (12)$$

202 *a. Incorporating Moist Energy into the Lorenz cycle*

212 As in Brown et al. (2023), we split the energy cycle of the MQG system into three parts: (1)
 213 kinetic energy, proportional to $|\vec{u}_1|^2 + |\vec{u}_2|^2$, (2) APE, proportional to $|\eta|^2$ and (3) ME, proportional
 214 to $|\eta_c|^2$. A modified Lorenz cycle for the energetics of the MQG system, constructed conceptually
 215 from exchanges between zonal mean and eddy flow, is depicted schematically in Figure 2. The
 216 classic dry Lorenz cycle is contained above the dot-dashed line. A zonally averaged APE is
 217 determined by the prescribed meridional gradient of the interface, $\bar{\eta}_y = -U\lambda^{-2}$. Downgradient
 218 mixing generates EAPE at rate ε_{APE} and converts it into EKE through vertical motion \mathcal{W} and
 219 lost at large scales due to Ekman dissipation \mathcal{D}_E . In a full Lorenz cycle, EKE would cascade to
 220 larger scales, ultimately generating a zonally averaged ZKE profile which reduces the ZAPE by
 221 redistributing the large-scale meridional temperature gradient. Because a background state ZKE
 222 is not prescribed in our homogeneous QG setup, these components are included only for reference
 223 via the dashed arrows.

224 The ME component, below the dashed line, accounts for the generation of latent heat release.
 225 We construct the domain-averaged EKE equation by multiplying Equations (1) and (2) by their
 226 respective streamfunction perturbation, averaging, and taking the sum. We construct the domain-
 227 averaged dry EAPE equation by multiplying Equation (3) by the interface perturbation η' and
 228 a constant $g^*/2H$ and the domain-averaged EME equation by multiplying Equation (4) by the
 229 condensation level perturbation η'_c and a constant $g^*(\mu_s - 1)/2H$. This yields

$$\partial_t \text{EKE} = +\mathcal{W} - \mathcal{D}_r \quad (13)$$

$$\partial_t \text{EAPE} = +\varepsilon_{APE} - \mathcal{W} + \mathcal{P} \quad (14)$$

$$\partial_t \text{EME} = +\varepsilon_{ME} - \mathcal{P} - \mathcal{D}_{ME} - \mathcal{D}_P \quad (15)$$

230 The terms in Equations (13) to (15) are defined in Table 1. The EKE receives injections from
 231 vertical motions \mathcal{W} near the Rossby deformation radius and dissipates energy at the largest scales
 232 through the Ekman term \mathcal{D}_E . The injections from vertical motions resolve anomalies in the APE.
 233 The anomalies are generated from the meridional sensible heat flux ε_{APE} and precipitation injection
 234 \mathcal{P} . The key modification from the dry cycle is in the precipitation term \mathcal{P} , which converts ME into
 235 APE.

236 As in Brown et al. (2023), the ME is constructed based on a quadratic of the condensation
 237 thickness so as to isolate the precipitation term in the energetics. EME is generated by the
 238 condensation thickness flux ε_{ME} . Like the sensible heat flux, this term redistributes the planetary
 239 scale gradient of the condensation thickness. At full saturation, MQG systems fully convert the
 240 condensation thickness flux into EAPE through precipitation. We will show that partially saturated
 241 systems convert only a portion of the same flux into EAPE. We include two terms for the loss of
 242 EME: \mathcal{D}_{ME} and \mathcal{D}_P . The first is a proxy for the small-scale diffusion of moisture, given by

$$\mathcal{D}_{ME} = \frac{g^* (\mu_s - 1)}{2H} \nu \overline{|\nabla^4 \eta'_c|^2}. \quad (16)$$

243 In equilibrated dry systems where moisture is a passive tracer, this is the only means of removing
 244 EME. As an eighth-order diffusion term, this term dominates at small scales. Small-scale diffusion
 245 is therefore largest in flows where a strong forward cascade results in substantial convergence of
 246 moisture to scales smaller than the deformation radius. In the saturated case, this term is negligible
 247 because precipitation terminates the forward cascade at scales larger than the diffusion scale (Brown
 248 et al. 2023).

249 In partially saturated systems, EME experiences an *eddy precipitation dissipation* of the form

$$\mathcal{D}_P = \frac{g^*}{2H} \overline{\mathcal{L}P'(\eta'_c - \eta')}. \quad (17)$$

250 The nonlinearity of the precipitation term complicates the impact of this dissipation on the EME,
 251 as precipitation only occurs in the regions where the eddy surplus exceeds the mean deficit, i.e.,

$$\eta'_c - \eta' > \eta_0 - \eta_{c,0}. \quad (18)$$

252 The eddy surplus is thus constrained by

$$\eta'_c - \eta' \leq \frac{\tau P}{1+C} - \eta_{c,0} + \eta_0, \quad (19)$$

EKE	$\overline{(u_1'^2 + u_2'^2)}/2$	Eddy Kinetic Energy
EAPE	$g^* \overline{ \eta' ^2}/2H$	Eddy Available Potential Energy
EME	$g^* (\mu_s - 1) \overline{ \eta_c' ^2}/2H$	Eddy Moist Energy
\mathcal{D}_r	$r \overline{ u_2'^2 }$	Ekman Dissipation
\mathcal{W}	$f_0 \overline{W' \eta'}/H$	APE to EKE Injection (Vertical Motion)
ε_{APE}	$-g^* \overline{\eta_y v_2' \eta'}/2H$	Sensible Heat Flux
ε_{ME}	$-g^* (\mu_s - 1) \overline{\eta_y v_2' \eta_c'}/2H$	Condensation Thickness Flux
\mathcal{P}	$g^* \overline{\mathcal{L} P' \eta'}/2H$	ME to APE Injection (Precipitation)
\mathcal{D}_{ME}	$g^* (\mu_s - 1) \nu \overline{ \nabla^4 \eta_c' ^2}/2H$	High-order diffusion
\mathcal{D}_P	$g^* \overline{\mathcal{L} P' (\eta_c' - \eta')}/2H$	Precipitation dissipation

TABLE 1. Generation, transfer, and dissipation terms for the Kinetic Energy and Moist Available Potential Energy.

253 Because equality occurs in precipitating regions, we multiply both sides by the precipitation P and
254 take the domain average to obtain

$$\overline{P' (\eta_c' - \eta')} = \frac{\tau \overline{P'^2}}{1+C} + \frac{\tau P_0^2}{1+C} - P_0 (\eta_{c,0} - \eta_0) \quad (20)$$

255 To determine the sign of this term, let us consider the perturbation and domain average terms
256 separately. The first term on the right-hand side is a quadratic of the precipitation anomaly and
257 only removes EME. The domain average of Equation (19) implies that the remaining terms are in
258 combination greater than zero, making \mathcal{D}_P a sink of EME.

259 In both the dry and saturated limit, \mathcal{D}_P vanishes. In the dry limit, there is no precipitation,
260 and therefore no precipitation dissipation. In the saturated limit, the assumption of instantaneous
261 precipitation adjustment $\tau \rightarrow 0$ renders the contribution of eddy precipitation negligible. Further-
262 more, Equation (19) is an equality, so the domain average of the remaining terms vanishes. In
263 partially saturated systems, precipitation changes the structure of the moisture content by selec-
264 tively flattening positive anomalies, resulting in an asymmetric reduction in moisture variance and
265 a shift to a larger average moisture deficit. Precipitation dissipation accounts for this suppression
266 of variance and corresponding adjustment to the mean moisture content.

267 *b. Dry and Saturated Limits*

268 The above dynamical system has two limiting cases. In the dry limit, moisture acts as a passive
269 tracer, mixed by turbulent dynamics to a diffusion scale. In the saturated limit, strong evaporation
270 and fast precipitation adjustment times results in a system that is raining everywhere and rapidly

271 adjusts the moisture profile to the saturation value set by the Clausius-Clayperon relation. The dry
 272 limit can be achieved under the condition $E = 0.0$ with a sufficiently long simulation time. Brown
 273 et al. (2023) showed that the saturated limit is achieved in this system in the limit of sufficiently high
 274 evaporation ($E = 1000U^2m_0/f_0\lambda^2$) and fast precipitation relaxation time ($\tau = 0.00125\lambda/U$). This
 275 saturated limit behaved as the dry limit with shorter length and faster time scales, characterized
 276 by powers of μ_s . Hence the saturated system has a significant increase in EKE, faster growth, and
 277 smaller scale instability compared with the dry case. In both cases, downgradient heat fluxes are
 278 converted into EKE with near perfect efficiency.

279 Partially saturated systems exhibit reduced mechanical output compared with both saturated and
 280 dry systems. The dissipation terms described in the previous section, which were negligible in the
 281 saturated case, become quite significant in the partially saturated case. We explore the transition
 282 from the dry limit to the saturated by considering systems with intermediate evaporation rates,
 283 so that precipitation occurs, but only locally. This localization creates a non-linearity such that
 284 moisture is neither a fully passive tracer (as in the dry case) nor correlated with temperature (as in
 285 the saturated case). We expect the partially saturated case to act as a combination of the dry and
 286 saturated cases. We explore the transition from the dry to the saturated limit and how the efficiency
 287 and mean moisture content of the system change through tuning the evaporation rate.

288 *c. Numerical Experiments*

289 The experiments bridge the gap between the moisture gradient sweeps in the partially saturated
 290 (Lapeyre and Held 2004) and saturated (Brown et al. 2023) cases. We fix the moisture and
 291 temperature gradients while varying the evaporation rate E to tune the degree of saturation, i.e.
 292 the portion of the domain that is supersaturated. Increasing the evaporation rate also increases the
 293 domain-averaged relative humidity of the system.

294 Experiments are done on the same system as in Brown et al. (2023). A complete list of
 295 the nondimensional parameters used is in Table 2, with E indicating the nondimensionalized
 296 evaporation and E^* the dimensional parameter. The domain size is $L = 18\pi\lambda$, with timesteps of
 297 size $dt = 0.00025\lambda/U$. Small-scale dissipation $\nu = 10^{-7}\lambda^7U$ is chosen to avoid damping small-
 298 scale energy generation associated with moist effects on the scales of instability. The precipitation
 299 timescale $\tau = 5dt$ is chosen to enforce rapid adjustment, and Ekman damping $r = 0.16U\lambda^{-1}$ is in

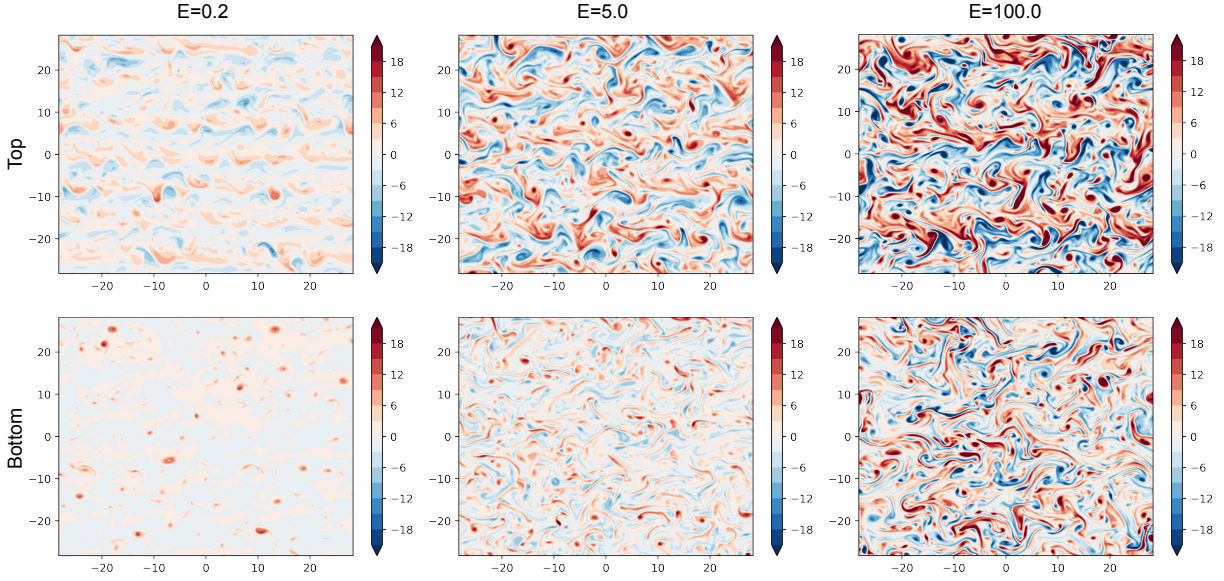
Parameter	Expression	Realistic	Represents	Simulation Values
ξ	$\frac{U}{\beta\lambda^2}$	1	Dry Criticality	0.8, 1.0, 1.25
μ_s	$\frac{1+C\mathcal{L}}{1-\mathcal{L}}$	$\approx 1.75 - 2.62$	Gross Moist Stability	1.75, 2.62, 4
E	$\frac{f_0\lambda^2}{U^2m_0}E^*$	0.4	Evaporation Rate	$(0, 1, 2, 5) \times (10^{-1}, 10^0, 10^1, 10^2)$
\mathcal{R}	$\frac{r\lambda}{U}$.16	Ekman damping	.16
τ^*	$\frac{\tau U}{\lambda}$	$< .15 - .85$	Precipitation timescale	0.00125
L/λ	L/λ	N/A	Domain size	18π
dt	$\frac{\Delta t U}{\lambda}$	N/A	Timestep	0.00025
ν^*	$U\lambda^7\nu$	N/A	Small scale dissipation	10^{-7}

316 TABLE 2. Tunable parameter space (nondimensionalized), realistic values, and the values used in the simula-
317 tions. Here, E^* is the dimensional evaporation parameter, and E is the nondimensionalized parameter.

300 line with the value used in e.g. Held and Larichev (1996). The values of the dry criticality ξ are
301 chosen to be near the realistic value of 1. The values of μ_s are informed by the range of realistic
302 season- and hemisphere-averaged values. We used simulations with $C = 2.0$ and $\mathcal{L} = .2, .35, .5$,
303 corresponding to $\mu_s = 1.75, 2.62, 4.0$. This roughly corresponds with a northern hemisphere winter,
304 northern hemisphere summer, and a higher moisture gradient. An additional run with $C = 0.0$ and
305 $\mathcal{L} = 0.75$ with $\mu_s = 4.0$ was performed to confirm that simulations with the same value of μ_s
306 behave similarly for the metrics we use. We chose the largest moisture gradient based on few
307 factors. First, on local scales, such as in the warm sector of surface cyclones (e.g., Emanuel
308 1985), latent heat release can fully overcome the dry static stability of the atmosphere, i.e. $\mathcal{L} \rightarrow 1$,
309 $\mu_s \rightarrow \infty$. Second, moisture gradients are expected to increase in warmer climates. Third, idealized
310 models corresponding to $\mu_s > 3.33$ have exhibited a transition to a vortex-dominated regime (e.g.,
311 Kohl and O’Gorman 2022), so steeper moisture gradients may correspond with a different regime
312 of instability. The evaporation is widely varied for the purposes of a parameter sweep, ranging
313 from an essentially dry case ($E=0.0$) to a value that is nearly saturated in all of our experiments
314 ($E=100.0$). Tuning the evaporation rate also tunes the rate of radiative cooling, maintaining the
315 energy balance at large scales.

318 4. On the Efficiency of Conversion of ME to KE by Precipitation

319 In midlatitude systems, both sensible and latent heat are mixed downgradient by eddy fluxes.
320 This results in a distribution of both across a wide range of scales. A key feature distinguishing the



323 FIG. 3. Snapshots of the top and bottom layer vorticity for $\xi = 0.8$, $\mu_s = 4.0$, with varying evaporation (labeled
 324 in each column).

321 impact of latent heat from sensible heat is that not all of the water vapor content of the atmosphere
 322 is condensed, and therefore only a portion of the latent heat transport ultimately impacts EKE.

325 In MQG, tuning the evaporation rate also controls the portion of displaced water vapor that is
 326 converted into sensible heat. Figure 3 shows the impact of this change in simulations with $\xi = 0.8$,
 327 $\mu_s = 4.0$. At low evaporation ($E = 0.2$), the upper-level flow is organized into seven narrow jets,
 328 while the low-level flow exhibits a few intense cyclonic vortices amidst a backdrop of weak PV
 329 anomalies. At high evaporation ($E = 5.0$), the upper-level flow organizes itself into five jets and the
 330 low-level flow begins to exhibit nearer symmetry in the distribution of cyclonic and anticyclonic
 331 extremes. The saturated limit is approached in the limit of extreme evaporation ($E = 100.0$). The
 332 upper-level flow organizes into three jets and the low-level flow features a number of extreme
 333 cyclone and anticyclone anomalies.

334 Figure 4 shows the time and domain averaged EKE as a function of evaporation rate for the
 335 full range of parameter sweeps. As a broad trend, EKE increases with the evaporation rate. Near
 336 $E = 10$, EKE converges to a maximum value for the experiments where $\xi = 1.25$, $\mu_s = 1.75$ and
 337 $\xi = 0.8$, $\mu_s = 1.75, 2.62$, corresponding to the transition to the saturated limit. We expect that a
 338 similar convergence would occur for all moisture and temperature gradients at sufficiently high

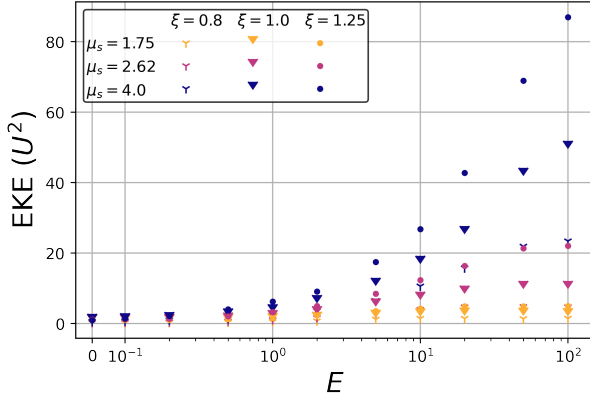


FIG. 4. The total EKE of the system as a function of evaporation.

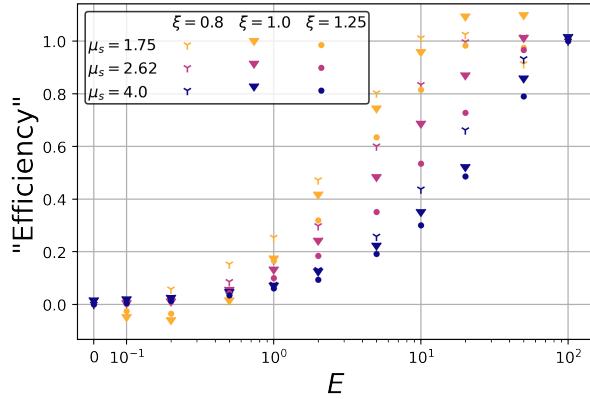


FIG. 5. An empirical estimate for the mechanical efficiency as a function of evaporation.

339 evaporation. This reflects the notion that a more turbulent atmosphere acts as a more efficient
 340 atmospheric dehumidifier. Consequently, systems with a lower saturated criticality $\mu_s \xi$ require a
 341 lower evaporation rate to achieve saturation. The saturation value of E appears to depend more
 342 strongly on the moisture gradients, characterized by μ_s , than on the dry temperature gradient,
 343 characterized by ξ .

344 In each set of evaporation sweeps, EKE increases significantly from the dry limit to the $E = 100$
 345 experiment. The systems with the steepest moisture gradients feature the greatest increase by a
 346 factor of ~ 100 . The sweep with $\xi = 1.25$, $\mu_s = 1.75$ features the smallest increase in EKE with
 347 evaporation rate, by a factor of ~ 3 . If we define the saturated limit studied in Brown et al. (2023) as
 348 the limit of perfect efficiency in a moist system, then the mechanical output of a partially saturated
 349 system relative to the saturated limit can be used as a way to assess how efficiently ME is converted

350 into Kinetic Energy. As a crude metric for the moist efficiency, we compare the EKE with the
 351 value in the "dry" and "saturated" limits, i.e.

$$\text{"Efficiency"} = \frac{\text{EKE} - \text{EKE}_0}{\text{EKE}_{100} - \text{EKE}_0}. \quad (21)$$

352 Here, EKE_0 is the EKE at $E = 0$ and EKE_{100} is the EKE at $E = 100$, holding the temperature
 353 and moisture gradients constant. Figure 5 shows the distribution of this metric as a function of
 354 evaporation. By definition, this metric enforces zero efficiency in the dry limit and perfect efficiency
 355 in the $E = 100$ limit. However, evaporation alone is not sufficient to predict the efficiency of a
 356 moist system. The amount of evaporation needed to achieve near-perfect efficiency increases with
 357 both the temperature and moisture gradients. Furthermore, a few of the systems with low moisture
 358 gradients ($\mu_s = 1.75, \xi = 1.0, 1.25$) exhibit a negative "efficiency" in the low evaporation, indicating
 359 a reduction in EKE relative to the dry limit. These results emphasize that impact of changes to the
 360 surface latent heat flux depend on the temperature and moisture structure.

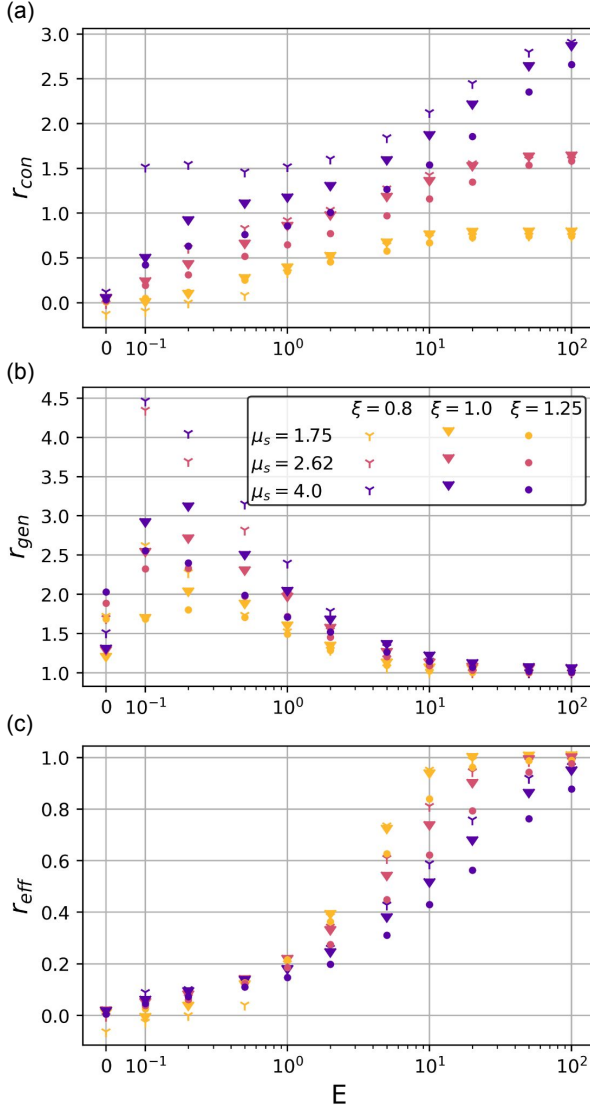
361 5. Generation, loss and conversion of Moist Available Potential Energy

362 We now characterize the moist conversion efficiency of a geostrophic system. Per the energetic
 363 framework of Section 3a, we identify three processes pertaining to latent heat in the atmosphere:
 364 (1) the *conversion* from EME to EAPE through precipitation, (2) the *generation* of ME through
 365 the meridional flux of sensible and latent heat, and (3) the *loss* of EME through diffusion and
 366 precipitation dissipation. For the first, we use a conversion ratio,

$$r_{\text{con}} = \frac{\langle \mathcal{P} \rangle}{\langle \mathcal{E}_{APE} \rangle}. \quad (22)$$

367 Parker and Thorpe (1995) and Moore and Montgomery (2005) argued that baroclinic growth
 368 dominates in systems where this ratio is much less than one, while diabatic effects dominate when
 369 the ratio is greater than one. In MQG, the conversion ratio goes to zero in the dry limit

$$\lim_{E \rightarrow 0} r_{\text{con}} = 0$$



373 FIG. 6. (a) The conversion ratio $r_{\text{con}} = \langle \mathcal{P} \rangle / \langle \varepsilon_{APE} \rangle$, (b) the generation ratio $r_{\text{gen}} = D_m / D_d =$
 374 $\langle \varepsilon_{APE} + \varepsilon_{ME} \rangle / \mu_s \langle \varepsilon_{APE} \rangle$, (c) the moist conversion efficiency $r_{\text{eff}} = \langle \mathcal{P} \rangle / \langle \varepsilon_{ME} \rangle = r_{\text{con}} / (\mu_s r_{\text{gen}} - 1)$, all ver-
 375 sus evaporation constant E .

370 In the saturated limit, Brown et al. (2023) showed that this ratio converges to

$$\lim_{E \rightarrow \infty} r_{\text{con}} = \mu_s - 1. \quad (23)$$

371 As a starting point in our discussion of the non-kinetic energetics, we explore how the conversion
 372 ratio changes with surface evaporation rate.

376 Figure 6a plots the conversion ratio as a function of evaporation. In the saturated limit, this
377 ratio converges as predicted to $\mu_s - 1 \approx 1.62$ and 0.75 for $\mu_s = 2.62$ and 1.75 , respectively, but
378 does not reach the predicted value of 3.0 for $\mu_s = 4.0$, consistent with these systems remaining
379 only partially saturated even for very high evaporation rate. Between the saturated and dry limits,
380 precipitation accounts for a gradually increasing portion of the APE generation, with the largest
381 increases typically occurring between the dry $E = 0$ case and the $E = 0.1$ case with a small injection
382 of moisture. This transition is sharpest in the case with sub-critical baroclinicity and high moisture
383 gradient ($\xi = 0.8$, $\mu_s = 4.0$), where only a small evaporation rate results in precipitation accounting
384 for $\sim 60\%$ of the APE generation. In comparison, the same evaporation rate and moisture gradients
385 in the $\xi = 1.25$ case results in a system with precipitation accounting for $\sim 30\%$ of the APE
386 generation. The $\xi = 1.0$ case has an evaporation dependency more similar to the $\xi = 1.25$ case
387 for small E , indicating that the presence of even a small amount of moisture has a much more
388 significant effect under conditions that would be stable in a dry simulation.

389 This large increase in conversion ratio in the low baroclinicity, high moisture ($\xi = 0.8$, $\mu_s = 4.0$)
390 experiment is reminiscent of the results of Kohl and O’Gorman (2022), whereby Diabatic Rossby
391 Vortices were found to exhibit the greatest unstable growth in the presence of weakened potential
392 vorticity gradients with a sufficient reduction in static stability. An equivalent configuration in MQG
393 would predict the strongest Diabatic Rossby Vortices for $\mu_s > 3.33$, $\xi < 1.0$. It is possible that
394 such a mechanism contributes to the sharp increase in conversion ratio at a low evaporation rates.
395 Indeed, the low level vorticity shown in Figure 3 exhibits isolated vortices that are qualitatively
396 consistent with this interpretation.

397 The generation of both APE and ME relates to the downgradient transport of sensible and latent
398 heat. In a dry system, this is characterized by the turbulent diffusivity of the sensible heat across
399 the inertial range of the inverse cascade, which directly predicts the total generation of EKE (e.g.,
400 Held and Larichev 1996). This concept can be extended for any quantity that acts as a passive
401 tracer within an inertial range (Smith et al. 2002). In the MQG system, we define the dry diffusivity

402 D_d and moist diffusivity D_m by

$$D_d = \frac{\overline{v'q'_{bc}}}{\overline{q_{bc_y}}} = \frac{\langle \varepsilon_{APE} \rangle}{U\lambda^{-2}g^*/2H} \quad (24)$$

$$D_m = \frac{\overline{v'_2q'_m}}{\overline{q_{m_y}}} = \frac{\langle \varepsilon_{APE} + \varepsilon_{ME} \rangle}{\mu_s U\lambda^{-2}g^*/2H}. \quad (25)$$

403 Here, v' represents the meridional barotropic velocity anomaly and q_{bc} represents the baroclinic
 404 potential vorticity. The moist potential vorticity q_m is defined as in Lapeyre and Held (2004) as a
 405 combination of the lower-level vorticity, the interface position and the condensation thickness. We
 406 define a generation ratio as the ratio between the diffusivity for moist potential vorticity and that
 407 of the dry potential vorticity:

$$r_{\text{gen}} = \frac{D_m}{D_d} = \frac{\langle \varepsilon_{APE} + \varepsilon_{ME} \rangle}{\mu_s \langle \varepsilon_{APE} \rangle}. \quad (26)$$

408 Figure 6b plots the generation ratio as a function of evaporation rate. In the saturated limit, this
 409 ratio converges to 1, indicating that humidity and temperature have proportionate diffusivity at
 410 saturation. At lower evaporation rates, the moist diffusivity is much higher than the dry diffusivity,
 411 increasing until near the dry limit. This portion increases as the dry criticality ξ decreases, and
 412 as the moisture gradient parameter μ_s increases, peaking at either $E = 0.1$ or $E = 0.2$ in all tested
 413 configurations. Systems with low evaporation ($0.0 < E < 0.5$), low baroclinicity ($\xi = 0.8$), and
 414 high moisture gradients ($\mu_s \geq 2.62$) exhibit substantially higher generation ratios, indicating that
 415 latent heat accounts for a large portion of the heat transport in these systems. At higher evaporation
 416 rates, the configuration of the flow changes to a more wavelike pattern, consistent with an increase
 417 in baroclinicity, enhanced by moisture. Indeed, a possible explanation for the high conversion
 418 ratio at low evaporation is isolated diabatic vortices that do not contribute much to the barotropic
 419 energy cascade, and consequently do not drive an increase in the sensible heat flux. As evaporation
 420 increases, more frequent diabatic forcing generates an elongated cascade, strengthening the moist
 421 baroclinicity of the system.

422 The low evaporation cases present an interesting contrast: even though they are very efficient at
 423 moving moisture, as characterized by the generation ratio r_{gen} , this enhanced moisture transport
 424 does not result in a large increase in the generation of kinetic energy, as measured by the low value
 425 of the conversion ration r_{con} . We further quantify this discrepancy in terms of a moist conversion

426 efficiency r_{eff} , capturing the portion of EME converted into EAPE, as the ratio of the precipitation
 427 conversion to the total EME generation by the meridional flux:

$$r_{\text{eff}} = \frac{\langle \mathcal{P} \rangle}{\langle \varepsilon_{ME} \rangle} = \frac{r_{\text{con}}}{\mu_s r_{\text{gen}} - 1}. \quad (27)$$

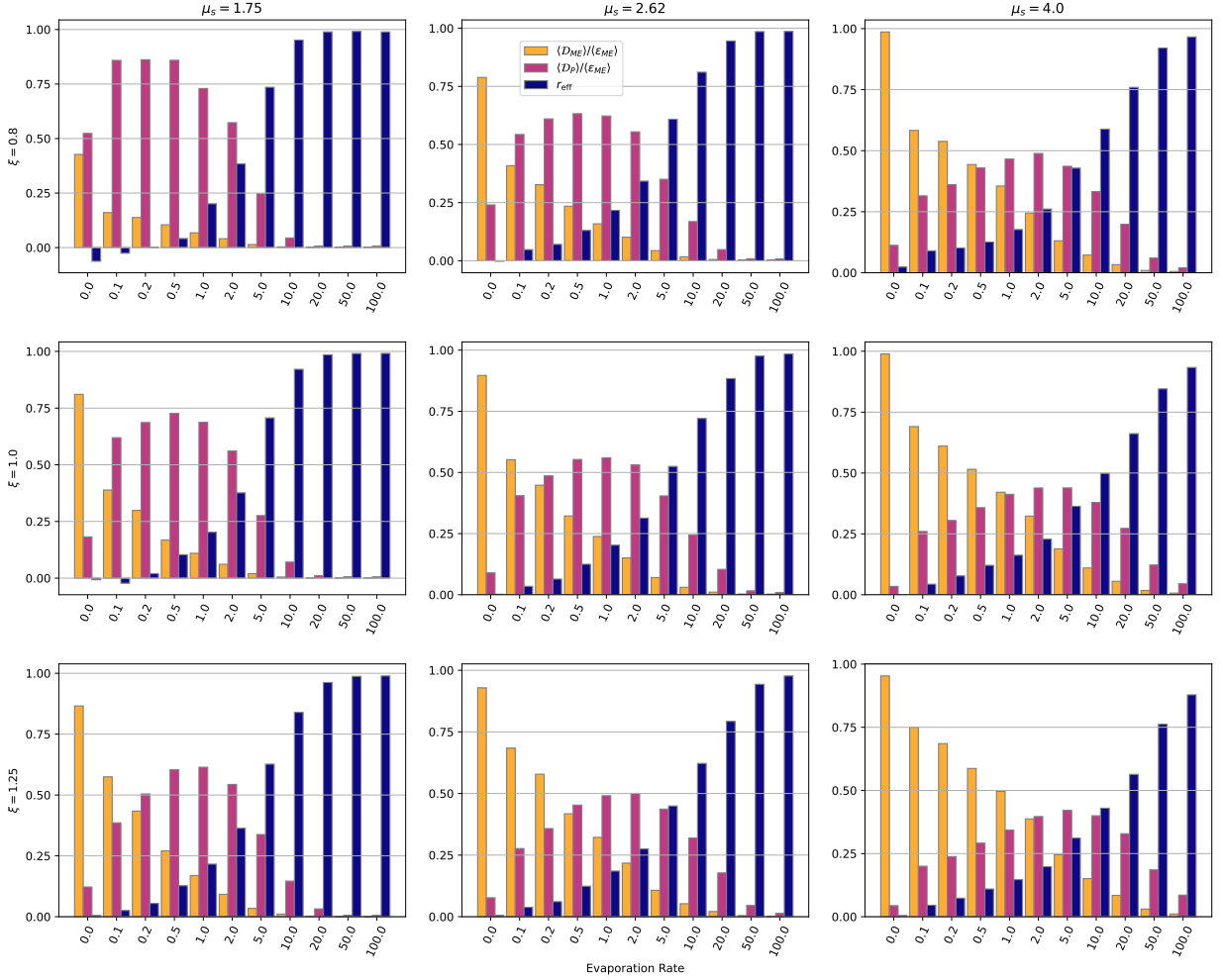
428 This loss ratio captures the transition from dry to moist geostrophic turbulence most dramatically,
 429 as it gradually increases from 0 - meaning that most of the EME is never converted into EKE -
 430 to 1 in the saturated limit, where all the EME is converted into EKE. In a few cases with low
 431 evaporation and low moisture gradients, this term is negative, indicating that precipitation has a
 432 net negative effect on the APE. This feature distinguishes the moist conversion efficiency from
 433 traditional metrics of mechanical efficiency.

434 The results of Figure 6b and c indicate that in partially saturated systems, only a fraction of the
 435 EME is converted into APE. Equation (15) indicates that the generation of EME by the meridional
 436 energy transport ε_{ME} is additionally removed through:

- 437 1. Small-scale diffusion of moisture \mathcal{D}_{ME} , which dominates in dry turbulent systems
- 438 2. Eddy precipitation dissipation \mathcal{D}_P , which occurs in partially saturated systems

442 Figure 7 shows the time-and-domain-averaged values of each sink term and the moisture conver-
 443 sion efficiency across the range of experiments. At the dry limit, moisture acts as a passive tracer in
 444 most of the domain, and hence the small scale diffusion \mathcal{D}_{ME} dominates in removing ME, except
 445 in subcritical systems which never fully equilibrate (e.g. $\xi = 0.8$, $\mu_s = 1.75$). For some simulations
 446 with low evaporation (e.g. $\xi = 0.8$, $\mu_s = 1.75$ and $E = 0.1$), precipitation acts as a small source of
 447 ME and sink of APE. Typically, precipitation acts as a sink of APE at larger scales, arising from
 448 the tendency for the poleward transport of moisture to produce precipitation poleward of the jet
 449 and flatten the temperature gradient. Crucially, the small-scale diffusion \mathcal{D}_{ME} requires sufficiently
 450 strong turbulence for the cascade to mix anomalies in the condensation thickness to the diffusion
 451 scale.

452 All but the most turbulent simulations ($\xi = 1.0, 1.25, \mu_s = 4.0$) converge to nearly perfect efficiency
 453 in the limit of high evaporation. Furthermore, systems with smaller temperature and moisture
 454 gradients converge to the saturated limit at lower evaporation rates, e.g. around $E = 20.0$ for the



439 FIG. 7. The portion of generated EME lost to (a) small-scale diffusion (light orange bars, left), (b) precipitation
 440 dissipation (pink bars, middle), and (c) the moisture conversion efficiency r_{eff} , which captures conversion to APE
 441 via precipitation (dark blue bars, right).

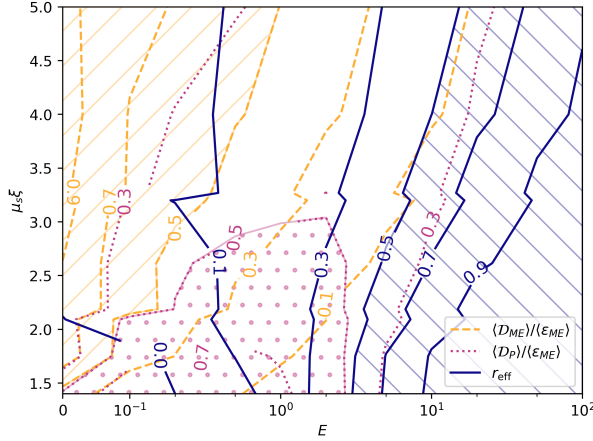
455 $\xi = 0.8$, $\mu_s = 1.75$ case. Because a more turbulent system is a more efficient dehumidifier, they
 456 require a larger injection of moisture in order to achieve full saturation.

457 The precipitation dissipation, \mathcal{D}_P , is a significant sink of EME at intermediate evaporation rates.
 458 This is most significant in the simulations that are subcritical in the dry scenario, where \mathcal{D}_P
 459 accounts for $\sim 90\%$ of the loss in the $\xi = 0.8$, $\mu_s = 1.75$, $E = 0.1, 0.2$ simulations. For evaporation
 460 sweeps at higher dry criticality with $\mu_s = 1.75$, precipitation dissipation is strongest at higher
 461 evaporation rates ($E = 0.5$ and $E = 1.0$ for $\xi = 1.0, 1.25$, respectively) and accounts for a smaller
 462 portion of the EME loss ($\sim 70\%$ and 60% for $\xi = 1.0, 1.25$, respectively). A similar shift occurs

463 when increasing moisture gradients. In the simulation with the steepest moisture and temperature
464 gradients ($\xi = 1.25$, $\mu_s = 4.0$), the peak occurs at $E = 5.0$ and accounts for only 40% of the
465 energy loss. Small-scale diffusion compensates for the reduction, and consequently the moisture
466 conversion efficiency is also smaller than simulations with the same evaporation but shallower
467 temperature and moisture gradients.

468 Eddy precipitation dissipation also accounts for why low baroclinicity ($\xi = 0.8$), low evaporation
469 ($0.0 < E < 0.5$) simulations have significantly different conversion ratios despite similar generation
470 ratios. In particular, precipitation dissipation accounts for more than half of the loss of EME when
471 $\mu_s \leq 2.62$. For the $\mu_s = 4.0$ simulations, precipitation dissipation is smaller and moisture conversion
472 efficiency is larger, with small-scale diffusion as the dominant source of inefficiency. This indicates
473 that precipitation dissipation plays a significant role in regulating the scale distribution of moisture
474 in the atmosphere. With steeper moisture gradients, small meridional displacements of moist air
475 generate highly localized latent heat release within a domain that is largely sub-saturated. This
476 allows for moisture to be mixed to small scales, further favoring localized latent heat release. In
477 systems with shallower moisture gradients, moisture must be transported further before latent heat
478 is released. In systems with steeper temperature gradients, baroclinic instability increases the
479 downgradient flux of sensible heat, decreasing both the conversion and generation ratios.

486 Figure 8 plots isolines of each mechanism for EME loss as a function of evaporation and ef-
487 fective saturated criticality. Small-scale diffusion tends to dominate at high saturated criticality,
488 low evaporation. Precipitation dissipation dominates at lower saturated criticality and intermediate
489 evaporation. Isolines of small-scale diffusion are steepest at low evaporation and become more
490 shallow as evaporation increases. Isolines of precipitation dissipation are steepest at low evapo-
491 ration and between $E = 2$ and $E = 5$, with a region of intermediate evaporation where the slope
492 of isolines is near zero. Moisture conversion efficiency is negative at low evaporation, with the
493 transition to positive between $E = 0.0$ and $E = 0.2$. Latent heat release therefore becomes a net
494 sink of APE in this region of parameter space. For larger values of E , isolines of precipitation have
495 a shallower slope with increasing E .



480 FIG. 8. Approximate isolines of the relative contribution of each possible EME sink as a function of the
 481 saturated criticality $\mu_s \xi$ and evaporation parameter E . In the hatched regions, a single process accounts for
 482 more than half of the EME loss. Small-scale diffusion (yellow) dominates at low evaporation a high saturated
 483 criticality. Precipitation dissipation (pink) dominates at intermediate evaporation and low saturated criticality.
 484 Moisture conversion efficiency (blue) approaches 1 at very high evaporation, with more evaporation required for
 485 higher saturated criticality.

496 6. Discussion

497 Let us define three regimes based on the moisture conversion efficiency and the dominant
 498 mechanism generating inefficiency:

- 499 1. Regime 1, a "dry-like" regime corresponding to low evaporation rates and higher saturated
 500 criticality. Here, small-scale diffusion \mathcal{D}_{ME} dominates the loss of ME and the system has low
 501 moist conversion efficiency. In Figure 8, this occurs in the yellow-hatched regions.
- 502 2. Regime 2, corresponding to intermediate evaporation rates and lower saturated criticality.
 503 Here, \mathcal{D}_P dominates the loss of ME and the system has intermediate moist conversion effi-
 504 ciency. In Figure 8, this occurs in the dotted pink region. There is a point above that line near
 505 $E = 2$, $\mu_s \xi = 3.27$ that also satisfies this condition.
- 506 3. Regime 3, a "saturated-like" regime corresponding to high evaporation. Here, almost all
 507 generated EME is converted into EAPE through precipitation \mathcal{P} . The system is therefore
 508 highly efficient at converting moisture into EKE. In Figure 8, the system approaches this limit
 509 in the blue-hatched region.

510 There are additionally regions where all three mechanisms significantly contribute. These are
511 marked without any hatching. In these regions, we expect to see features of all three regimes, with
512 the distribution depending on the relative size of each contribution.

513 To gain insight into the dynamical implications of each regime, we modify turbulence theory to
514 take into account the non-linearity of precipitation. If moisture behaves purely as a passive tracer
515 (as is nearly achieved in Regime 1), the turbulent flow mixes moisture downgradient, generating
516 variance in the moisture deficit. A more turbulent flow, corresponding to a higher value of ξ ,
517 generates larger variance due to the stronger forward cascade. This accounts for the diagonal tilt of
518 the lines delineating different regimes. Because this "dry-like" regime allows the forward cascade
519 of moisture to continue to the diffusion scale without precipitation disrupting the cascade near the
520 Rossby scale (not shown), there is a large variance in the moisture distribution down to very small
521 scales. This regime thus favors small scale precipitation anomalies that lead to vortices like those
522 found in the left column of Figure 3.

523 In Regime 2, precipitation dissipation becomes the dominant sink of EME. The condensa-
524 tion process selectively removes moisture surpluses, introducing skewness to the distribution and
525 decreasing the mean and variance moisture deficit. This regime contains many instances of precip-
526 itation having a negative contribution to the EAPE and a positive contribution to the EME. A large
527 precipitation dissipation term more than counteracts the positive forcing of precipitation in the
528 EME, and thus precipitation in this regime results in a loss of EAPE without a corresponding gain
529 in EME. In Regime 3, the system begins to behave more similarly to the saturated limit discussed in
530 Brown et al. (2023), with precipitation-driven exchanges between the EME and EAPE dominating.

531 *a. Turbulent Mixing and Relative Humidity*

532 The energetic output of MQG is governed by an interplay between the generation of moisture
533 variance by turbulent processes and its removal by moist processes. The reduced impact of moisture
534 diffusion in more saturated systems demonstrates that precipitation halts the forward cascade if the
535 availability of moisture allows it. We use this observation in conjunction with turbulence theory
536 to demonstrate how the moisture conversion efficiency relates to the relative humidity.

537 Let us assume that the moisture deficit is Gaussian in its distribution, with mean value

$$d_0 = \langle \eta_{c,0} - \eta_0 \rangle, \quad (28)$$

538 and a variance

$$\sigma_d = \left\langle (\eta'_c - \eta')^2 \right\rangle^{1/2}, \quad (29)$$

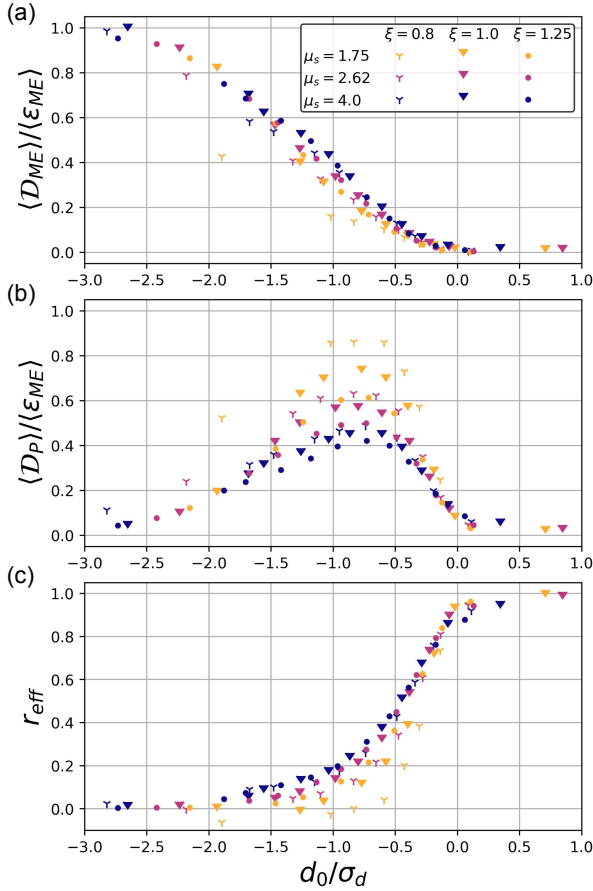
539 defined by the RMS deficit perturbation. Condensation occurs in the regions where $\eta_c - \eta > 0$. We
540 estimate this portion of the domain by $\alpha \approx \int_0^\infty \phi(x, d_0, \sigma_d) dx$, where $\phi(x, d_0, \sigma_d)$ is the normal
541 distribution of the deficit x with mean value d_0 and standard deviation σ_d . Intuitively, the value of
542 this portion of the domain is dependent on a distribution parameter d_0/σ_d , with a smaller portion
543 of the domain at saturation for more negative values of d_0/σ_d .

547 Figure 9 demonstrates that the dominant mechanism of EME loss is strongly correlated with the
548 distribution parameter d_0/σ_d . At $d_0/\sigma_d = 0$, the system transitions from a mean deficit to a mean
549 surplus. Regime 1 occurs for values smaller than ~ -1.5 , Regime 2 peaks between -1 to -0.5 , and
550 Regime 3 begins to dominate for values larger than -0.2 . While the relative size of the precipitation
551 and small-scale diffusion largely converge in value for similar values of the distribution parameter,
552 the precipitation dissipation exhibits a wide range of peak values. Smaller moisture and temperature
553 gradients are both correlated with relatively larger precipitation dissipation. Indeed, the systems
554 with the largest moisture gradients ($\mu_s = 4.0$) never lose a majority of the EME to precipitation
555 dissipation, and instead occupy a regime where all three sinks are of comparable size. In contrast,
556 the simulations with the smallest moisture gradients ($\mu_s = 1.75$) lose over 80% of their EME to
557 precipitation dissipation. In a few small μ_s simulations, precipitation has only a small positive or
558 net negative effect on the EAPE.

559 The dynamical features of MQG are therefore determined by the size of the mean moisture
560 deficit relative to the RMS deficit variance. The moisture deficit is the counterpart of the relative
561 humidity, which is thus correlated with the moisture conversion efficiency (Figure 9c).

562 *b. Climate Estimates for the Evaporation Constant*

563 We now turn to the question of where current and future climates fall within the parameter space
564 of Figure 8. Lapeyre and Held (2004) estimate that a realistic parameter range is near $E = 0.4$,



544 FIG. 9. The fractional loss of EME due to (a) small-scale diffusion, (b) domain-scale diffusion, and (c)
 545 precipitation conversion as a function of the ratio between mean deficit and the RMS deficit variance. Panel (c)
 546 is equivalent to the moisture conversion efficiency.

565 $\mu_s \xi \in (1.75, 2.62)$ bounded by average winter and summer limits, respectively. Estimating changes
 566 under warming is difficult due to feedbacks between moist and dry processes. Nonetheless, we can
 567 synthesize the results of a few studies for a qualitative prediction of changes to the non-dimensional
 568 evaporation parameter.

569 The evaporation constant E is defined as

$$\begin{aligned} E &= \frac{f_0 \lambda^2}{U^2 m_0} E^* \\ &= \frac{E^*}{m_0} \cdot \frac{\lambda^2 \beta}{U} \cdot \frac{f_0}{\beta U} \\ &= \frac{1}{\tau_E} \cdot \frac{1}{\xi} \cdot \tau_\zeta. \end{aligned} \quad (30)$$

570 In the third line, we have decomposed this constant into three terms:

- 571 1. The first term is the inverse of an evaporation timescale $\tau_E = E^*/m_0$. Following Held and
572 Soden (2006), the evaporation rate E^* increases more slowly than Clausius-Clayperon, while
573 the typical moisture content m_0 scales with the Clausius-Clayperon relationship. In a warmer
574 climate, we therefore expect this term to decrease.
- 575 2. The second term is the inverse of the criticality for dry baroclinic instability. Stone (1978)
576 argues that the extratropical atmosphere adjusts to marginal criticality $\xi \approx 1$. If this remains the
577 case in a warmer world, we would expect the super-criticality to remain unchanged. However,
578 we note that this assumption neglects the impact of moist processes, which may generate
579 moist baroclinic adjustment under dry configurations that would otherwise be stable. In this
580 case, the criticality may decrease, slightly increasing E .
- 581 3. The last term is a vorticity advection timescale. Changes to this timescale are governed by
582 changes to the wind shear U . Shaw and Miyawaki (2024) argue that the impact of moisture
583 leads to an increase in the thermal wind, which predominantly impacts the fastest winds of
584 the jet stream. If this reflects global changes to the mean wind shear, this timescale should
585 decrease.

586 We would thus expect that in a warmer planet, the non-dimensional evaporation parameter de-
587 creases. This indicates that the midlatitude dynamics shifts toward a more "dry-like" regime and
588 to precipitation switching from a positive to negative impact on the EKE. The primary drivers
589 for this shift are the slowing down of the hydrological cycles (Held and Soden 2006) and the
590 intensification of the thermal wind (Shaw and Miyawaki 2024). However, a more detailed study
591 would be necessary to rigorously quantify the effect.

592 7. Conclusions

593 We demonstrated that the relative humidity of the atmosphere, as set by the surface evaporation
594 rate, can greatly impact the intensity of midlatitude eddies. Building upon the energetic framework
595 of Brown et al. (2023) for the MQG equations, we analyzed the sensitivity of the generation of
596 kinetic energy by geostrophic turbulence to the evaporation rate. We found that as evaporation
597 increases, moist geostrophic turbulence gradually transitions from a dry limit ($E \rightarrow 0$) characterized
598 by low level of kinetic energy to a saturated limit ($E \rightarrow \infty$) with much more intense turbulence.
599 At low evaporation rates, systems with shallower moisture gradients exhibit a reduction in total
600 energetic output compared with the dry limit, a result previously only shown in non-homogeneous
601 moist systems (e.g., Bembenek et al. 2020; Lutsko and Hell 2021). Systems with steeper moisture
602 gradients remain at roughly the same energetic output. Further increases in evaporation lead to
603 a rapid increase in EKE in all systems, with higher baroclinicity and steeper moisture gradients
604 corresponding to a more rapid increase (Figure 4). As each system approaches a saturated limit,
605 the energetic output levels off. Systems with higher baroclinicity and steeper moisture gradients
606 require more evaporation to reach this limit.

607 The generation of kinetic energy by moist geostrophic turbulence is tied to the meridional
608 transport of latent and sensible heat. By transporting moisture poleward, the eddies extract ME
609 from the background gradient and convert it into APE through precipitation. Critically, this
610 conversion is inefficient in that only a fraction of ME is converted to kinetic energy and becomes
611 increasingly efficient as evaporation increases, with all EME being converted into EKE in the
612 saturated limit. Simultaneously, stronger turbulent dynamics reduce the efficiency of conversion,
613 resulting in a tug-of-war on the total efficiency from competing processes of moisture availability
614 and turbulent mixing. We develop a concept of moist conversion efficiency by expanding upon
615 existing metrics characterizing the relative contribution of dry and moist processes: the conversion
616 ratio of Parker and Thorpe (1995) and a generation ratio that we define by the relative strength of
617 the moist static energy flux to the dry static energy flux.

618 The inefficient conversion of ME to kinetic energy arises from the fact that EME is dissipated
619 through small-scale diffusion and eddy-scale precipitation diffusion. The former dominates when
620 the system is sufficiently turbulent (driving the elongation of the forward cascade of ME) and
621 sufficiently dry (lest precipitation halt the cascade before the dissipation scale). The latter dominates

622 when the system is roughly balanced between regions of saturation and deficit, such that ME is
623 lost through both the selective flattening of surplus anomalies by precipitation and evaporation into
624 regions of deficit. We show that the dominant mechanism of ME loss is correlated with the ratio
625 of the mean moisture deficit to the RMS deficit variance, capturing the availability of moisture
626 relative to the strength of turbulent mixing. When the mean deficit is large compared to the variance
627 (with a ratio less than ~ -1.5), precipitation is sparse and highly localized, leading to a system
628 with mostly dry behavior but some localized storms. For ratios between -1 and -0.5, precipitation
629 becomes more widespread, leading to a regime dominated by precipitation dissipation. As this
630 ratio approaches 0, the crossover from a mean deficit to a surplus, the system approaches the
631 saturated limit and most of the ME is converted into APE.

632 Our results indicate that diabatic processes play a large role in setting the scale distribution
633 of energy in the atmosphere. Indeed, MQG may underestimate the size of that role. Notably,
634 precipitation dissipation $\mathcal{D}_P \propto \tau P^2$ vanishes in the limit $\tau \rightarrow 0$, which we studied here. A larger
635 precipitation relaxation would further decrease efficiency. Evaporation similarly dissipates EME.
636 This term disappears with uniform evaporation, but a surface flux evaporation would yield an
637 evaporation dissipation term of the form

$$\mathcal{D}_E \propto |U_2| d^2. \quad (31)$$

638 The effect of these additional dissipation terms is likely to lead to more reduction of the moisture
639 variance than found here, further correlating moisture and temperature.

640 While the MQG system is highly idealized, the impacts of relative humidity on the generation
641 of kinetic energy in geostrophic turbulence have also been noted in moist convection (Pauluis and
642 Held 2002a; Pauluis 2011; Singh and O’Gorman 2016), tropical cyclones (Pauluis and Zhang
643 2017) and the global circulation (Laliberté et al. 2015). Furthermore, the mathematical expression
644 for dissipation by diffusion and precipitation are highly similar to those for irreversible entropy
645 production entropy due to diffusion of water vapor and irreversible phase changes. These strongly
646 indicate that our findings are not an artifact of the MQG system, but reflect the physical sensitivity
647 of moist eddies to the relative humidity of the atmosphere.

648 Furthermore, we have defined metrics that can be calculated explicitly for a range of models
649 across the hierarchy of complexity. The generation ratio r_{gen} is computed from a ratio of the

650 meridional fluxes of moist and dry static energy flux combined with the gross moist stability of
651 Neelin and Held (1987). The moist conversion efficiency is defined by a combination of the
652 generation ratio and conversion ratio. Similarly, the ratio between mean moisture deficit and RMS
653 deficit variance is calculated from the difference between the saturation and absolute humidity.
654 This can be done both globally and on localized domains by computing the domain average and
655 RMS variance of the humidity deficit. The results of this study can therefore be verified and
656 connected to more complex models.

657 *Acknowledgments.* This research was supported in part by the US NSF through award OAC-
658 2004572 and the NYU IT High Performance Computing resources, services, and staff expertise.

659 *Data availability statement.* The code used to generate the data in this study is stored in the
660 repository at https://github.com/margueriti/Moist_QG_public.

661 **References**

662 Adames, F., and Y. Ming, 2018: Interactions between Water Vapor and Potential Vorticity in
663 Synoptic-Scale Monsoonal Disturbances: Moisture Vortex Instability. *Journal of the Atmo-*
664 *spheric Sciences*, **75** (6), 2083–2106, <https://doi.org/10.1175/JAS-D-17-0310.1>.

665 Barry, L., G. C. Craig, and J. Thuburn, 2002: Poleward heat transport by the atmo-
666 spheric heat engine. *Nature*, **415** (6873), 774–777, <https://doi.org/10.1038/415774a>, URL
667 <https://www.nature.com/articles/415774a>.

668 Bembenek, E., D. N. Straub, and T. M. Merlis, 2020: Effects of Moisture in a Two-Layer Model of
669 the Midlatitude Jet Stream. *Journal of the Atmospheric Sciences*, **77** (1), 131–147, [https://doi.org/](https://doi.org/10.1175/JAS-D-19-0021.1)
670 [10.1175/JAS-D-19-0021.1](https://doi.org/10.1175/JAS-D-19-0021.1).

671 Brown, M. L., O. Pauluis, and E. P. Gerber, 2023: Scaling for Saturated Moist Quasi-Geostrophic
672 Turbulence. *Journal of the Atmospheric Sciences*, <https://doi.org/10.1175/JAS-D-22-0215.1>,
673 URL [https://journals.ametsoc.org/view/journals/atsc/aop/JAS-D-22-0215.1/JAS-D-22-0215.1](https://journals.ametsoc.org/view/journals/atsc/aop/JAS-D-22-0215.1/JAS-D-22-0215.1.xml).
674 xml.

675 Chemke, R., Y. Ming, and J. Yuval, 2022: The intensification of winter mid-latitude storm
676 tracks in the Southern Hemisphere. *Nature Climate Change*, **12** (6), 553–557, [https://doi.org/](https://doi.org/10.1038/s41558-022-01368-8)
677 [10.1038/s41558-022-01368-8](https://doi.org/10.1038/s41558-022-01368-8), URL <https://www.nature.com/articles/s41558-022-01368-8>.

- 678 Emanuel, K. A., 1985: Frontal Circulations in the Presence of Small Moist Symmetric Sta-
679 bility. *Journal of the Atmospheric Sciences*, **42** (10), 1062–1071, [https://doi.org/10.1175/
680 1520-0469\(1985\)042<1062:FCITPO>2.0.CO;2](https://doi.org/10.1175/1520-0469(1985)042<1062:FCITPO>2.0.CO;2), URL [http://journals.ametsoc.org/doi/10.1175/
681 1520-0469\(1985\)042<1062:FCITPO>2.0.CO;2](http://journals.ametsoc.org/doi/10.1175/1520-0469(1985)042<1062:FCITPO>2.0.CO;2).
- 682 Emanuel, K. A., M. Fantini, and A. J. Thorpe, 1987: Baroclinic Instability in an Environment of
683 Small Stability to Slantwise Moist Convection. Part I: Two-Dimensional Models. *Journal of the
684 Atmospheric Sciences*, **44** (12), 1559–1573, [https://doi.org/10.1175/1520-0469\(1987\)044<1559:
685 BIIAEO>2.0.CO;2](https://doi.org/10.1175/1520-0469(1987)044<1559:BIIAEO>2.0.CO;2).
- 686 Frierson, D. M. W., 2006: Robust increases in midlatitude static stability in simula-
687 tions of global warming. *Geophysical Research Letters*, **33** (24), [https://doi.org/https://doi.
688 org/10.1029/2006GL027504](https://doi.org/https://doi.org/10.1029/2006GL027504), URL [https://agupubs.onlinelibrary.wiley.com/doi/abs/10.1029/
689 2006GL027504](https://agupubs.onlinelibrary.wiley.com/doi/abs/10.1029/2006GL027504).
- 690 Held, I. M., and V. D. Larichev, 1996: A Scaling Theory for Horizontally Homogeneous, Baro-
691 clinically Unstable Flow on a Beta Plane. *Journal of the Atmospheric Sciences*, **53** (7), 946–952,
692 [https://doi.org/10.1175/1520-0469\(1996\)053<0946:ASTFHH>2.0.CO;2](https://doi.org/10.1175/1520-0469(1996)053<0946:ASTFHH>2.0.CO;2).
- 693 Held, I. M., and B. J. Soden, 2006: Robust Responses of the Hydrological Cycle to Global
694 Warming. *Journal of Climate*, **19** (21), 5686–5699, <https://doi.org/10.1175/JCLI3990.1>, URL
695 <http://journals.ametsoc.org/doi/10.1175/JCLI3990.1>.
- 696 Juckes, M. N., 2000: The Static Stability of the Midlatitude Troposphere: The Rele-
697 vance of Moisture. *Journal of Atmospheric Sciences*, **57** (18), 3050–3057, [https://doi.org/
698 10.1175/1520-0469\(2000\)057<3050:TSSOTM>2.0.CO;2](https://doi.org/10.1175/1520-0469(2000)057<3050:TSSOTM>2.0.CO;2).
- 699 Kohl, M., and P. A. O’Gorman, 2022: The Diabatic Rossby Vortex: Growth Rate, Length
700 Scale, and the Wave–Vortex Transition. *Journal of the Atmospheric Sciences*, **79** (10),
701 2739–2755, <https://doi.org/10.1175/JAS-D-22-0022.1>, URL [https://journals.ametsoc.org/view/
702 journals/atsc/79/10/JAS-D-22-0022.1.xml](https://journals.ametsoc.org/view/journals/atsc/79/10/JAS-D-22-0022.1.xml).
- 703 Laliberté, F., J. Zika, L. Mudryk, P. J. Kushner, J. Kjellsson, and K. Döös, 2015: Constrained
704 work output of the moist atmospheric heat engine in a warming climate. *Science*, **347** (6221),

705 540–543, <https://doi.org/10.1126/science.1257103>, URL <https://www.science.org/doi/10.1126/science.1257103>.

706

707 Lambaerts, J., G. Lapeyre, and V. Zeitlin, 2011: Moist versus Dry Barotropic Instability in a
708 Shallow-Water Model of the Atmosphere with Moist Convection. *Journal of the Atmospheric
709 Sciences*, **68** (6), 1234–1252, <https://doi.org/10.1175/2011JAS3540.1>.

710 Lapeyre, G., and I. M. Held, 2004: The Role of Moisture in the Dynamics and Energetics
711 of Turbulent Baroclinic Eddies. *Journal of the Atmospheric Sciences*, **61** (14), 1693–1710,
712 [https://doi.org/10.1175/1520-0469\(2004\)061<1693:TROMIT>2.0.CO;2](https://doi.org/10.1175/1520-0469(2004)061<1693:TROMIT>2.0.CO;2).

713 Lever, M., and O. Pauluis, 2024: Entropy-conditioned Statistics Naturally Capture Tropical Con-
714 vection’s Moisture-Driven Response to Surface Warming. (*in review*).

715 Lorenz, D. J., and E. T. DeWeaver, 2007: Tropopause height and zonal wind response to
716 global warming in the IPCC scenario integrations. *Journal of Geophysical Research: At-
717 mospheres*, **112** (D10), 2006JD008 087, <https://doi.org/10.1029/2006JD008087>, URL [https://
718 //agupubs.onlinelibrary.wiley.com/doi/10.1029/2006JD008087](https://agupubs.onlinelibrary.wiley.com/doi/10.1029/2006JD008087).

719 Lutsko, N. J., and M. C. Hell, 2021: Moisture and the Persistence of Annular Modes. *Journal of
720 the Atmospheric Sciences*, **78** (12), 3951–3964, <https://doi.org/10.1175/JAS-D-21-0055.1>.

721 Moore, R. W., and M. T. Montgomery, 2004: Reexamining the Dynamics of Short-Scale, Diabatic
722 Rossby Waves and Their Role in Midlatitude Moist Cyclogenesis. *Journal of the Atmospheric
723 Sciences*, **61** (6), 754–768, [https://doi.org/10.1175/1520-0469\(2004\)061<0754:RTDOSD>2.0.
CO;2](https://doi.org/10.1175/1520-0469(2004)061<0754:RTDOSD>2.0.
724 CO;2).

725 Moore, R. W., and M. T. Montgomery, 2005: Analysis of an Idealized, Three-Dimensional
726 Diabatic Rossby Vortex: A Coherent Structure of the Moist Baroclinic Atmosphere. *Journal of
727 the Atmospheric Sciences*, **62** (8), 2703–2725, <https://doi.org/10.1175/JAS3472.1>.

728 Moore, R. W., M. T. Montgomery, and H. C. Davies, 2008: The Integral Role of a Diabatic Rossby
729 Vortex in a Heavy Snowfall Event. *Monthly Weather Review*, **136** (6), 1878–1897, [https://doi.org/
730 10.1175/2007MWR2257.1](https://doi.org/10.1175/2007MWR2257.1), URL <http://journals.ametsoc.org/doi/10.1175/2007MWR2257.1>.

- 731 Neelin, J. D., and I. M. Held, 1987: Modeling Tropical Convergence Based on the Moist Static En-
732 ergy Budget. *Monthly Weather Review*, **115** (1), 3–12, [https://doi.org/10.1175/1520-0493\(1987\)](https://doi.org/10.1175/1520-0493(1987)115(0003:MTCBOT)2.0.CO;2)
733 [115\(0003:MTCBOT\)2.0.CO;2](https://doi.org/10.1175/1520-0493(1987)115(0003:MTCBOT)2.0.CO;2).
- 734 O’Gorman, P. A., T. M. Merlis, and M. S. Singh, 2018: Increase in the skewness of extratrop-
735 ical vertical velocities with climate warming: fully nonlinear simulations versus moist baro-
736 clinic instability. *Quarterly Journal of the Royal Meteorological Society*, **144** (710), 208–217,
737 <https://doi.org/10.1002/qj.3195>, URL <https://onlinelibrary.wiley.com/doi/10.1002/qj.3195>.
- 738 O’Gorman, P. A., 2010: Understanding the varied response of the extratropical storm tracks
739 to climate change. *Proceedings of the National Academy of Sciences*, **107** (45), 19 176–
740 19 180, <https://doi.org/10.1073/pnas.1011547107>, URL [https://pnas.org/doi/full/10.1073/pnas.](https://pnas.org/doi/full/10.1073/pnas.1011547107)
741 [1011547107](https://pnas.org/doi/full/10.1073/pnas.1011547107).
- 742 Parker, D. J., and A. J. Thorpe, 1995: Conditional Convective Heating in a Baroclinic Atmosphere:
743 A Model of Convective Frontogenesis. *Journal of the Atmospheric Sciences*, **52** (10), 1699–1711,
744 [https://doi.org/10.1175/1520-0469\(1995\)052\(1699:CCHIAB\)2.0.CO;2](https://doi.org/10.1175/1520-0469(1995)052(1699:CCHIAB)2.0.CO;2).
- 745 Pauluis, O., 2011: Water Vapor and Mechanical Work: A Comparison of Carnot and Steam Cycles.
746 *Journal of Atmospheric Sciences*, **68** (1), 91–102, <https://doi.org/10.1175/2010JAS3530.1>.
- 747 Pauluis, O., and I. M. Held, 2002a: Entropy Budget of an Atmosphere in Radiative–Convective
748 Equilibrium. Part I: Maximum Work and Frictional Dissipation. *Journal of Atmospheric Sci-*
749 *ences*, **59** (2), 125–139, [https://doi.org/10.1175/1520-0469\(2002\)059\(0125:EBOAAI\)2.0.CO;2](https://doi.org/10.1175/1520-0469(2002)059(0125:EBOAAI)2.0.CO;2).
- 750 Pauluis, O., and I. M. Held, 2002b: Entropy Budget of an Atmosphere in Radiative–Convective
751 Equilibrium. Part II: Latent Heat Transport and Moist Processes. *Journal of Atmospheric Sci-*
752 *ences*, **59** (2), 140–149, [https://doi.org/10.1175/1520-0469\(2002\)059\(0140:EBOAAI\)2.0.CO;2](https://doi.org/10.1175/1520-0469(2002)059(0140:EBOAAI)2.0.CO;2).
- 753 Pauluis, O. M., and F. Zhang, 2017: Reconstruction of Thermodynamic Cycles in a High-
754 Resolution Simulation of a Hurricane. *Journal of the Atmospheric Sciences*, **74** (10),
755 3367–3381, <https://doi.org/10.1175/JAS-D-16-0353.1>, URL [https://journals.ametsoc.org/doi/](https://journals.ametsoc.org/doi/10.1175/JAS-D-16-0353.1)
756 [10.1175/JAS-D-16-0353.1](https://journals.ametsoc.org/doi/10.1175/JAS-D-16-0353.1).
- 757 Pavan, V., N. Hall, P. Valdes, and M. Blackburn, 1999: The importance of moisture distribution
758 for the growth and energetics of mid-latitude systems. *Annales Geophysicae*, **17** (2), 242–256,

759 <https://doi.org/10.1007/s00585-999-0242-y>, URL <https://angeo.copernicus.org/articles/17/242/>
760 1999/.

761 Schneider, T., and P. A. O’Gorman, 2008: Moist Convection and the Thermal Stratification
762 of the Extratropical Troposphere. *Journal of the Atmospheric Sciences*, **65** (11), 3571–3583,
763 <https://doi.org/10.1175/2008JAS2652.1>.

764 Shaw, T. A., and O. Miyawaki, 2024: Fast upper-level jet stream winds get faster under climate
765 change. *Nature Climate Change*, **14** (1), 61–67, <https://doi.org/10.1038/s41558-023-01884-1>,
766 URL <https://www.nature.com/articles/s41558-023-01884-1>.

767 Shaw, T. A., and Coauthors, 2016: Storm track processes and the opposing influences of climate
768 change. *Nature Geoscience*, **9** (9), 656–664, <https://doi.org/10.1038/ngeo2783>.

769 Singh, M. S., and P. A. O’Gorman, 2016: Scaling of the entropy budget with surface temperature
770 in radiative-convective equilibrium. *Journal of Advances in Modeling Earth Systems*, **8** (3),
771 1132–1150, <https://doi.org/10.1002/2016MS000673>, URL [https://onlinelibrary.wiley.com/doi/](https://onlinelibrary.wiley.com/doi/10.1002/2016MS000673)
772 [10.1002/2016MS000673](https://onlinelibrary.wiley.com/doi/10.1002/2016MS000673).

773 Smith, K. S., G. Boccaletti, C. C. Henning, I. Marinov, C. Y. Tam, I. M. Held, and G. K.
774 Vallis, 2002: Turbulent diffusion in the geostrophic inverse cascade. *Journal of Fluid Mechan-*
775 *ics*, **469**, 13–48, <https://doi.org/10.1017/S0022112002001763>, URL [https://www.cambridge.](https://www.cambridge.org/core/product/identifier/S0022112002001763/type/journal_article)
776 [org/core/product/identifier/S0022112002001763/type/journal_article](https://www.cambridge.org/core/product/identifier/S0022112002001763/type/journal_article).

777 Stone, P. H., 1978: Baroclinic Adjustment. *Journal of the Atmospheric Sciences*, **35** (4), 561–571,
778 [https://doi.org/10.1175/1520-0469\(1978\)035<0561:BA>2.0.CO;2](https://doi.org/10.1175/1520-0469(1978)035<0561:BA>2.0.CO;2).

779 Wernli, H., S. Dirren, M. A. Liniger, and M. Zillig, 2002: Dynamical aspects of the life cycle of the
780 winter storm ‘Lothar’ (24–26 December 1999). *Quarterly Journal of the Royal Meteorological*
781 *Society*, **128** (580), 405–429, <https://doi.org/10.1256/003590002321042036>, URL [http://doi.](http://doi.wiley.com/10.1256/003590002321042036)
782 [wiley.com/10.1256/003590002321042036](http://doi.wiley.com/10.1256/003590002321042036).

783 Whitaker, J. S., and C. A. Davis, 1994: Cyclogenesis in a Saturated Environment. *Journal of*
784 *the Atmospheric Sciences*, **51** (6), 889–908, [https://doi.org/10.1175/1520-0469\(1994\)051<0889:](https://doi.org/10.1175/1520-0469(1994)051<0889:CIASE>2.0.CO;2)
785 [CIASE>2.0.CO;2](https://doi.org/10.1175/1520-0469(1994)051<0889:CIASE>2.0.CO;2), URL [https://journals.ametsoc.org/view/journals/atsc/51/6/1520-0469_1994_](https://journals.ametsoc.org/view/journals/atsc/51/6/1520-0469_1994_051_0889_ciase_2_0_co_2.xml)
786 [051_0889_ciase_2_0_co_2.xml](https://journals.ametsoc.org/view/journals/atsc/51/6/1520-0469_1994_051_0889_ciase_2_0_co_2.xml).

787 Zurita-Gotor, P., 2005: Updraft/Downdraft Constraints for Moist Baroclinic Modes and Their
788 Implications for the Short-Wave Cutoff and Maximum Growth Rate. *Journal of the Atmospheric*
789 *Sciences*, **62** (12), 4450–4458, <https://doi.org/10.1175/JAS3630.1>.